PAPER

Preparation of high-quality graphene oxide-carbon quantum dots composites and their application for electrochemical sensing of uric acid and ascorbic acid

IOP Publishing Nanotechnology
Nanotechnology 32 (2021) 135501 (12pp) https://doi.org/10.1088/1361-6528/abd12a

Preparation of high-quality graphene oxide-carbon quantum dots composites and their application for electrochemical sensing of uric acid and ascorbic acid

Ling Ding[1,2,*], Huan He[1], Jin Zhou[1], Dini Wang[3], Qiong Nian[3,*], Shiqian Li[4], Shihui Qian[1], Wenbing Li[1], Cui Liu[2] and Zhengyong Liang[5]

[1] School of Chemistry and Chemical Engineering, Hubei Provincial Key Laboratory for New Processes of Ironmaking and Steel making, Wuhan University of Science and Technology, Wuhan 430081, People's Republic of China
[2] Key Laboratory of Optoelectronic Chemical Materials and Devices, Ministry of Education, School of Chemical and Environmental Engineering, Jianghan University, Wuhan 430056, People's Republic of China
[3] School of Engineering for Matter, Transport and Energy, Arizona State University, Tempe, AZ 85287, United States of America
[4] Key Laboratory of Measurement and Control System for Offshore Environment, Fuqing Branch of Fujian Normal University, Fuqing 350300, People's Republic of China
[5] Henan Provincial Engineering Laboratory of Coal-based Ecological Fine Chemicals, Zhengzhou 450001, People's Republic of China

E-mail: dingling@wust.edu.cn and qnian@asu.edu

Received 10 September 2020, revised 27 November 2020
Accepted for publication 7 December 2020
Published 8 January 2021

Abstract

Graphene oxide-quantum dots systems are emerging as a new class of materials that hold promise for biochemical sensing applications. In this paper, the eco-friendly carbon quantum dots (CQDs) are prepared with cheap and recyclable coke powders as carbon source. The graphene oxide-carbon quantum dots (GO-CQDs) composites are synthesized using graphene oxide as the conductive skeleton to load the CQDs by a one-step calcination method. The obtained GO-CQDs composites demonstrate the successful decoration of CQDs on GO nanosheets. The CQDs acting as spacers create gaps between GO sheets, resulting in a high surface area, which electively increases the electrolyte accessibility and electronic transmission. The electrocatalytic activity and reversibility of GO-CQDs composites can be effectively enhanced by tuning the mass ratio of GO to CQDs and the heating process. Furthermore, a highly sensitive and selective electrochemical sensor for determining uric acid (UA) and ascorbic acid (AA) was developed by modifying GO-CQDs composites onto a glassy carbon electrode. The results show that the linear range, minimum detection limit, and sensitivity of the GO-CQDs electrode for UA detection are 1–150 μM, 0.01 μM, and 2319.4 μA mM^{-1} cm^{-2}, respectively, and those for AA detection are 800–9000 μM, 31.57 μM, and 53.1 μA mM^{-1} cm^{-2}, respectively. The GO-CQDs are employed as the electrode materials for the serum and urine samples electrochemical sensing, the results indicate that the sensor can be used for the analysis of real biological samples.

Supplementary material for this article is available online

* Authors to whom any correspondence should be addressed.

Keywords: graphene oxide, carbon quantum dots, composite materials, electrochemical sensor, uric acid and ascorbic acid

(Some figures may appear in colour only in the online journal)

1. Introduction

Uric acid (UA) and ascorbic acid (AA) are important signaling molecules in human body fluids and closely related to human health. If the concentration of UA deviates away from the normal level, the functions of human cells will be affected, causing symptoms, such as scurvy, swollen, and painful gums [1]. In recent years, the detection of UA and AA is achieved using the capillary electrophoresis, high-performance liquid chromatography, and noble metal modified electrodes [2–4], etc. However, they are still limited by many aspects, such as the cumbersome instruments, complex pretreatment of samples, high cost, etc. Xie *et al* [5] reports that a polyaniline/reduced graphene oxide nanocomposite prepared by the hydrothermal method can be employed to detect dopamine (DA), however, it exhibits no obvious reaction to UA and AA. The recent literatures show that a hierarchical nano-porous PtTi sensor or a phytic acid/graphene oxide nanocomposites modified electrode can be used to detect DA, UA, and AA, but the sensitivity and detection limit need to be further improved [6, 7]. Therefore, it is of great significance to explore biosensors with high sensitivity, high selectivity, low detection limit, high repeatability, and simple operation in the medicine and analytical chemistry fields. Graphene, as a new type of two-dimensional carbon nanostructured material, has the advantages of large specific surface area (2600 $m^2\ g^{-1}$), high conductivity, high mechanical strength [8–10], etc. It can be used as the substrate material to enhance the electron conductivity, adsorption capacity, and catalytic activity of reactants in electrochemical biosensing. The defects and functional groups on graphene sheets can provide abundant active sites to improve the reaction thermodynamics and kinetics [11], while the direct use of bare graphene in biosensors shows no obvious property upgrade due to its like-metal-semiconductor nature of the zero-bandgap, high chemical stability, and an inert surface [12]. Moreover, the graphene nanosheets are apt to reunite in aqueous solution causing the decrease in the specific surface area and therefore affecting the binding sites for detection. This also leads to less active layer and higher internal resistance of graphene [13]. So, in order to improve the properties of graphene, we can construct the graphene-based composite material using the zero-dimensional nanomaterial, such as metal nanoparticles, metal oxide nanoparticles, quantum dots, etc. On one hand, the composite can combine the properties of both nanoparticles and graphene, and on the other hand, can bring more active sites due to the unique interaction between the two species [14–16].

Carbon quantum dots (CQDs) are zero-dimensional fluorescence nanomaterials. CQDs have advantages of tunable fluorescence emission, wider excitation wavelength, good light stability, mild chemical composition, and as well as simple synthesis and modification, lower cost [17, 18]. More importantly, CQDs have unique photoelectric properties and high specific surface area, and is nontoxic and cheap raw material when compared to some other zero-dimensional nanomaterials including metal nanoparticles, metal oxide nanoparticles, etc. The metal nanoparticles and metal oxide nanoparticles are significantly more expensive than CQDs. Furthermore, CQDs can be used in a variety of applications such as electronic, photoluminescence, electrochemical and electrochemiluminescence sensor [19–21], etc. Due to the novel properties of CQDs, sensors based on CQDs can achieve a high level of performance. Sun *et al* [22] focused on sensors and analytical systems that utilize CQDs as a key component. Dong *et al* [23] used CQDs as nucleating and anchoring points to facilitate the formation of highly dispersed Pt nanoparticles on RGO. Apart from the function of anchoring points, CQDs as spacers also can retard restacking of RGO sheets and support abundant oxygen groups to improve the material antipoisonous performance. So the CQDs can be well combined with inorganic and organic materials to improve their properties. To obtain the large accessible surface area, high active interface, and unique local electron distribution, GO can be integrated with CQDs to form the GO-CQDs composites by loading CQDs on the surface of GO. The three-dimensional composite structure constituted by both GO and CQDs can enhance the electron transfer rate and surface electrochemical activity on the electrode interface. This can also facilitate the full contact between electrolyte and electrode to improve the electrochemical activity of the electrode and the sensitivity of electrode detection. Although some progress have been made, it is still urgent to synthesize high quality and excellent sensing properties graphene-QDs composite by an easy synthesis method with inexpensive raw materials. Therefore, our group has explored the preparation method of GO-CQDs and biochemical sensing applications.

In this study, the eco-friendly CQDs are prepared with cheap and recyclable coke powders as carbon source. Then we prepared the GO-CQDs composite by a one-step calcination and characterized the morphology and structure of the composite with various techniques. The effects of calcination temperature, reaction time, and GO-to-CQDs mass ratio on the structure and properties of GO-CQDs composites are investigated, to find the optimum synthesis conditions of the GO-CQDs composites. In addition, the electrochemical activity and cyclic stability of the composite were studied by electrochemical tests. To demonstrate the application potential of GO-CQDs composites in biosensors for the detection of UA and AA, the sensitivity and minimum detection limit of the GO-CQDs electrode were measured and calculated, respectively, providing a reference for the construction of electrochemical sensors for the efficient molecule detection.

2. Experimental and methods

2.1. Raw materials

Coke powders were obtained from Wuhan Iron and Steel Limited Co. of China. Graphite powders with a purity of 98.0 wt% were obtained from Qingdao Tianheda Graphite co. Ltd. The concentrations of sulfuric acid, nitric acid, and hydrochloric acid were 98.0, 65.0, and 37.0 wt%, respectively. All the chemicals were of analytical pure, and the water used throughout the experiments was deionized. Fresh human serum and urine fluid samples were provided by the Hospital of Wuhan University of Science and Technology, China. Informed consent was obtained from the human subject.

2.2. Synthesis and purification of CQDs

The coke powders (0.1 g) were first pretreated by grinding, sieving, and drying and then added into a three-flask with a mixture of concentrated H_2SO_4 (12 ml) and HNO_3 (4 ml). The mixture was stirred and heated at 100 °C for 8 h and adjusted to maintain a desired pH value of 10. Then, the mixture solution was dialyzed for two days in ultrapure water (the cut-off of the dialysis membrane is equal to a molecular weight of 3000) to remove salts and purified by centrifugation in acetone and isopropanol. Finally, these CQDs samples were dissolved in Tris-HCl buffer solution and stored at 4 °C.

2.3. Preparation of GO-CQDs

The used GO was synthesized by chemical oxidation according to an improved Hummers' method [24]. GO-CQDs composites were prepared using GO as the conductive skeleton to load CQDs by a one-step calcination method. Various combinations of the calcination temperature, time, and GO-to-CQDs mass ratio (m_{GO}:m_{CQDs}) were used in preparation to obtain the electrode materials with optimized electrochemical properties. The GO-CQDs composites with excellent electrochemical activity could be prepared when the mass ratio of GO:CQDs, heating reaction temperature, and reaction time were 50:1, 150 °C, and 120 min, respectively.

In this case, the as-prepared GO samples (500 mg) were grinded into powder, and then ultra-sonically dispersed in 6 ml of CQDs solution for 30 min. Subsequently, the uniform mixture of GO and CQDs was casted into a reaction kettle and heated in a muffle furnace at 150 °C for 120 min. After the reaction was finished, the kettle was naturally cooled to room temperature. The GO-CQDs composites were obtained by centrifugation at the speed of 9000 rpm for 15 min. The resulting products were washed with deionized water and dried at 60 °C for 12 h.

2.4. Structural characterization

The surface morphologies of GO and GO-CQDs composites were characterized by field-emission scanning electron microscopy (SEM, FEI Nova 400 Nano). Transmission electron microscopy (TEM) was carried out on a JEM-2100UHR (JEOL, Japan) with an accelerating voltage of 200 kV. The structural properties were characterized by Fourier-transform infrared spectroscopy (FT-IR, VERTEX 70), Raman spectroscopy, and x-ray diffraction (XRD, X pert Pro MPD). The optical properties were characterized by a UV spectrophotometer (UV–vis, U-3010). Raman spectra of GO and GO-CQDs composites excited by the He–Cd laser at a wavelength of 325 nm. The electrochemical properties were measured by an electrochemical workstation (CHI660C). Measurements of electrochemical signal responses under different preparation and application conditions were performed repeatedly. Each result was expressed as the average of three reduplicate measurements.

2.5. Electrochemical test

The electrochemical properties of GO and GO-CQDs composites were measured using a three-electrode cell. The counter and reference electrodes were a platinum wire and a Ag/AgCl electrode, respectively. The glassy carbon electrode (GCE) modified with the GO-CQDs composite was used as the working electrode. The GCE was first polished with Al_2O_3 slurries (0.05 μm) to obtain a mirror-like surface and washed ultrasonically in ethanol water (1:1, v/v ratio) solution and deionized water for 15 min, respectively. Then, the GCE was air-dried at room temperature. The GO-CQDs composite powder (1.0 mg) was completely dispersed in deionized water (1.0 ml). After that, the obtained dispersion (10.0 μl) was dropped to the GCE and air-dried at room temperature.

To evaluate the reversibility and cyclic stability of the GO-CQDs electrode, the cyclic voltammograms (CVs) and electrochemical impedance spectra (EIS) of the GO-CQDs/GCE working electrode were measured in a mixture of 5 μM $K_3Fe(CN)_6$ and 1 M KCl.

To test the GO-CQDs electrode as the selective electrochemical biosensor for the detection of UA and AA, the CV curves was measured in the 0.1 M phosphate buffer solution (PBS, pH = 7.4), the 0.1 M PBS with 1 mM AA, the 0.1 M PBS with 0.1 mM UA, and the 0.1 M PBS with 1 mM AA and 0.1 mM UA. The differential pulse voltammetry (DPV) diagram of the GO-CQDs electrode was measured in 0.1 M PBS containing UA with concentrations of 0.1–150 μM and 1 mM AA. The amperometric current–time responses curves of the GO-CQDs electrode were measured under the continuous addition of UA with concentrations of 0.1–150 μM or AA with concentrations of 800–9000 μM in 0.1 M PBS at a voltage of 0.4 V.

3. Results and discussion

3.1. Characterization of materials

The SEM and TEM images of the as-prepared pure GO, CQDs and GO-CQDs composites were shown in figure 1. The pure GO (figure 1(a)) exhibits crumpled structures with apparent interlayer stacking and surface folding. The morphology of the GO-CQDs composite (figure 1(b)) is similar to that of pure GO, but without observable stacking. The SEM image of the

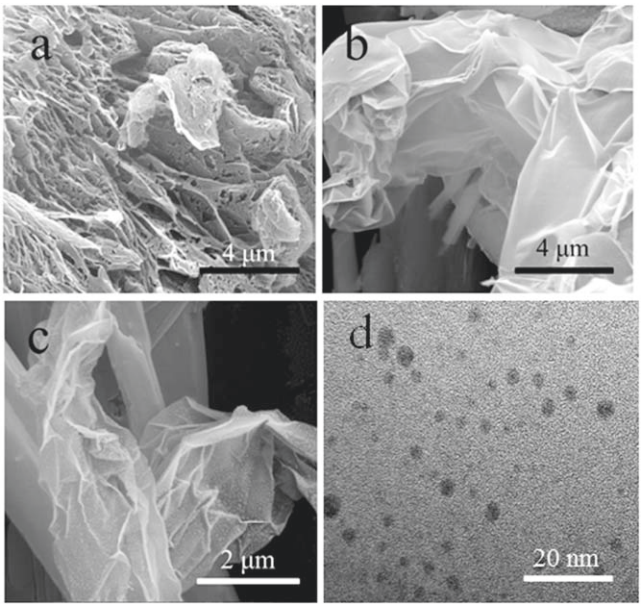

Figure 1. SEM images of (a) GO and (b,c) GO-CQDs composites; (d) TEM micrographs of CQDs.

GO-CQDs composite at a higher magnification (figure 1(c)) shows the fine particles on the surface of the GO, demonstrating the successful loading of CQDs with the size about 2–5 nm (figure 1(d)) on the GO nanosheets to form GO-CQDs composites.

The GO-CQDs composites maintain the original flake structure of GO and avoid restacking issue, which might attribute to CQDs acting as surface modifiers change the GO flake surface energy or as spacers create gaps and alleviate restacking of GO sheets [23, 25]. Whereas, a high specific surface area can be achieved, which can further electively increase the electrolyte accessibility and ionic transportation. Additionally, the addition of CQDs may also be expected to increase the mechanical strength of GO according to previous studies [26, 27].

Figure 2 shows the XRD patterns of graphene and GO-CQDs composites. As shown in figure 2(a), the characteristic peak of graphite (001) appears at 10.7°. The calculated interlayer spacing of GO using Bragg formula is 0.828 nm, wider than that of the original graphite layer (0.335 nm). Larger space is introduced between the GO layers, resulting in the absence of electrons in the conjugated system of carbon layers.

Figure 2(b) shows that the diffraction peak of GO-CQDs composites appears at 24.2°. The interlayer spacing of GO-CQDs composites is calculated to be 0.367 nm. Compared with bare GO, the lamellar spacing of the composites decreases by 55.8%. The CQDs, as the electron donor, may compensate the lack of electrons on the GO layers, decreasing the interlayer space and increasing the mechanical strength.

Figure 3 is the Raman spectra of GO and GO-CQDs composites excited by the He-Cd laser at a wavelength of 325 nm. The two most distinct bands in Raman spectra of graphene materials are the G band at 1580 cm^{-1} and the D band at 1340 cm^{-1}. The G band reflects the in-plane vibration of sp^2-hybridized carbon atoms on an ordered graphite structure. The D band is attribute to the out-of-plane vibration of the disordered sp^3 hybrid carbon atoms, and its peak strength is mainly affected by the number of defect sites [28]. Figure 3(a) shows that the D and G peaks corresponding to 1340 and 1588 cm^{-1} are close to the theoretical value. Furthermore, the intensity ratio of the D to G band (I_D:I_G) is larger than 1, indicating that there are many oxygen-containing functional groups, holes, and defects on the surface of GO. Figure 3(b) shows the D and G peaks of GO-CQDs composites at 1340 and 1583 cm^{-1} are close to the theoretical values as well, but their intensity ratio decreases (I_D:$I_G \approx 1$). This may due to the fact that, after the surface of GO is loaded with CQDs, the number of holes and defect sites of GO decreases so that the intensity of the D band weakens, while that of G band is still strong. This indicates that the interaction between GO layers is enhanced and the degree of graphitization is improved, which weakens the stacking between GO layers and improves the specific surface area of GO. Furthermore, in figure 3(b), a distinct peak is observed at 732 cm^{-1}, indicating the existence of CQDs. This is because the functional group of CQDs can induce the external bending vibration of Ar–H (four adjacent hydrogen atoms) [29].

The FT-IR spectra of GO and GO-CQDs composites (figure 4(a)) display the peaks at 3425 (–OH stretching vibration), 2920, 2850 (C(sp^3)–H stretching vibration), 1640 (C=C stretching vibration), and 1450 cm^{-1} (C–H in-plane bending vibration). This indicates that the variety of functional groups on the GO surface does not decrease after the loading of CQDs, so the composite will retain the original chemical properties of GO. Additional absorption peaks were observed in the composite at 2000 (asymmetry C≡C stretching vibration), 1030 (C(sp^3)–O stretching vibration), 875 (Ar–H external bending vibration), 605, and 565 cm^{-1} (terminal alkyne ≡C–H external bending vibration). Some of these groups belong to the CQDs, while others are newly formed due to the incorporation of GO and CQDs, indicating that the two materials are connected by chemical bonds during the calcination. Moreover, it also shows that the composite not only has the structural characteristics of GO but also owns the excellent properties of CQDs, which are beneficial to the performance of material in biochemical sensing.

The UV–vis spectra of GO and GO-CQDs composites (figure 4(b)) both have strong absorption peaks in the wavelength range of 220–240 nm, causing by a $\pi \rightarrow \pi^*$ transition. The absorption peak of the composite blue-shifts about 14 nm compared to that of GO, suggesting the decrease of conjugated length on the composite. The reason may attribute to the fact that some conjugated regions composed of C=C double bonds in GO are transformed to C–C single bonds after graphene is loaded with CQDs.

3.2. Effect of synthesis conditions on GO-CQDs composites

The reversibility of the electrode plays a vital role in electrochemical biosensing, and that of the GO-CQDs electrode can be significantly affected by the synthesis conditions. As

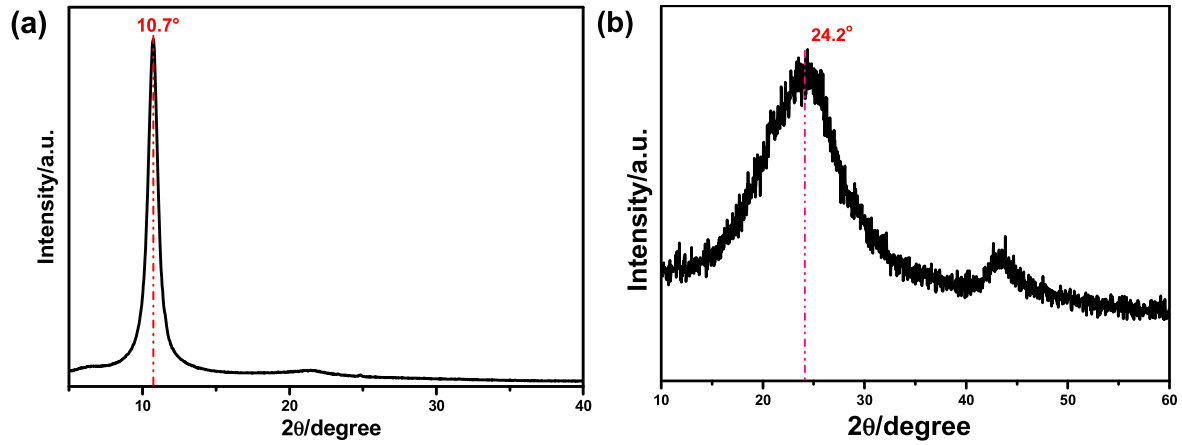

Figure 2. XRD patterns of (a) GO and (b) GO-CQDs composites.

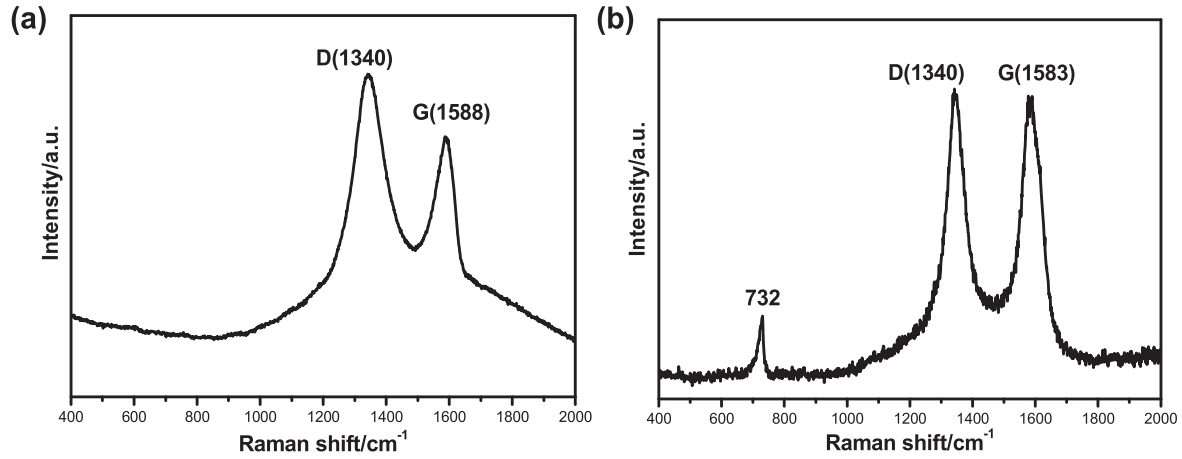

Figure 3. Raman spectra of (a) GO and (b) GO-CQDs composites.

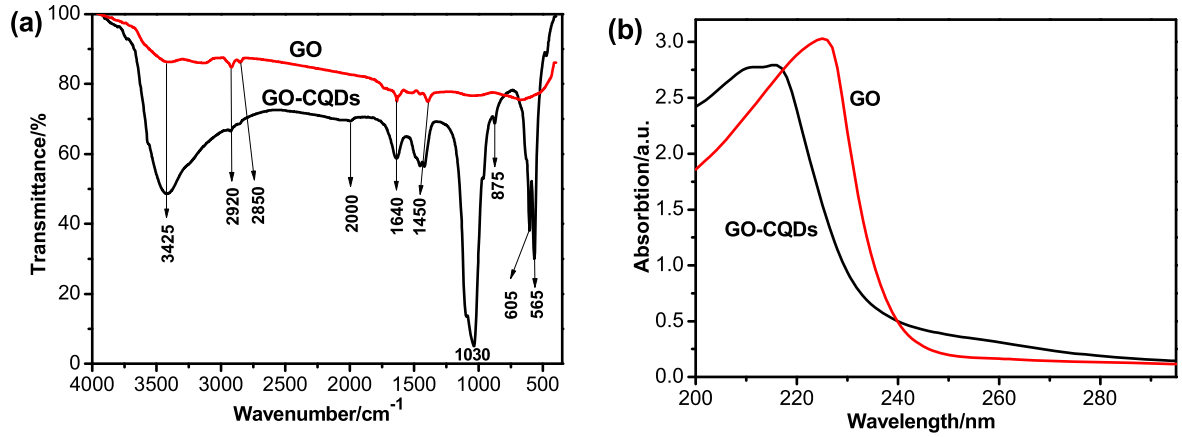

Figure 4. (a) FT-IR spectra of GO and GO-CQDs; (b) UV–vis spectra of GO and GO-CQDs.

shown in figure 5(a), the peak-to-peak potential (ΔE_P) of the GO-CQDs electrode changes obviously with the nine different synthesis conditions. The ΔE_P values of the nine GO-CQDs electrodes change apparently, suggesting that the reversibility of the GO-CQDs electrode varies with the synthesis conditions. Distinct redox peaks between 0.2 and 0.4 V have been observed for all the nine GO-CQDs electrodes, while an alignment of the reversible peak on the curve indicates a certain degree of cyclic stability and reversibility been retained. The ratios of anodic-to-cathodic peak current (i_{pa}:i_{pc}) of the nine GO-CQDs electrodes are all close to 1, and the maximum is only 1.03, indicating that the electrode system is quasi-reversible, and the electrode has outstanding electrochemical activity.

Figure 5(b) shows the relationship between m_{GO}:m_{CQDs} and ΔE_P. When m_{GO}:m_{CQDs} = 50:1, the GO-CQDs electrode

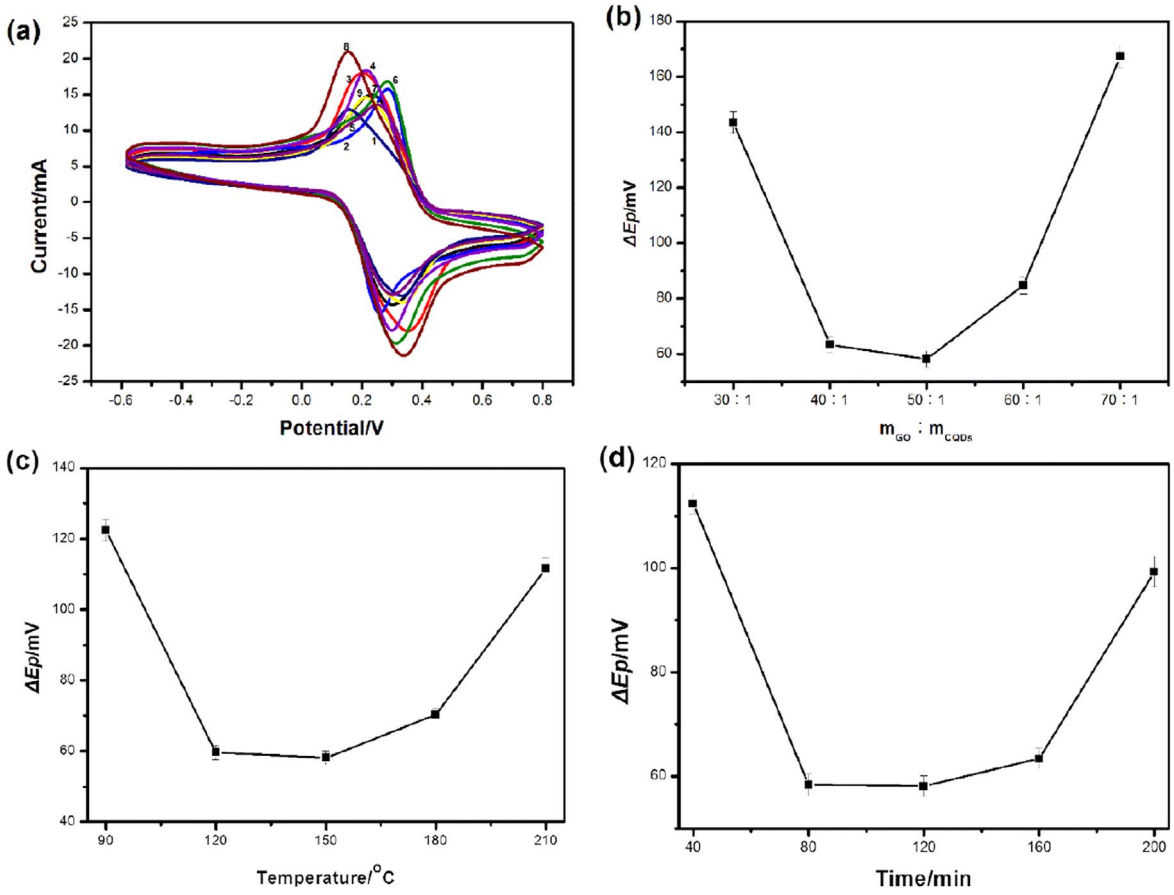

Figure 5. (a) CV of nine GO-CQDs electrodes in a mixture of 5 μM $K_3Fe(CN)_6$ and 1 M KCl with a scan rate of 100 mV s^{-1}; (b) relationship between m_{GP}:m_{CQDs} and ΔE_P; (c) relationship between calcination temperature and ΔE_P; (d) relationship between calcination time and ΔE_P.

shows the minimum ΔE_P of 58.1 mV. Larger or smaller m_{GO}:m_{CQDs} causes a significant increase of ΔE_P. Whether the electron transfer rate of material is enhanced or not, which can be determined by comparing the peak-to-peak potential. With a low percentage of CQDs, the electron transfer rate cannot be sufficiently enhanced, so the improvements of detection rate and sensitivity will be limited for these GO-CQDs electrodes. Excessive loading of CQDs also hinders the electron transport and reduces the efficiency of electrochemical sensing.

Figure 5(c) plots the ΔE_P of the GO-CQDs electrodes with different calcination temperatures. When the calcination temperature is between 120 °C and 150 °C, the ΔE_P swings from 58.1 to 59.6 mV, showing that the calcination temperature in this range has slight impact on the reversibility of the electrodes. However, when the calcination temperature is lower than 120 °C, the reversibility of the electrode reduces drastically. This is because the calcination temperature is not high enough to provide the enough binding energy required for CQDs to load on the graphene surface. Most of GO nanosheets and CQDs still separate from each other. The catalytic performance of CQDs is weakened, which can be determined by comparing the peak-to-peak potential. When the calcination temperature is higher than 180 °C, a series of reactions can degrade and destroy CQDs, resulting in a great weakening of the performance of CQDs as a catalyzer or sensitizer.

Figure 5(d) shows the relationship between the calcination time and ΔE_P. When the calcination time is 120 min, the ΔE_P reaches a minimum value of 58.1 mV. The calcination time between 80 and 160 min has no significant impact on the cyclic properties of the GO-CQDs electrodes. However, the calcination time shorter than 80 min or longer than 160 min levels ΔE_P up to exceeding 100 mV. Therefore, the calcination time should also be controlled between 80 and 160 min to obtain much better cyclic properties.

3.3. Electrochemical properties of GO and GO-CQDs composites

To further investigate the electrochemical properties of the GO-CQDs electrode and to compare it with the electrode made of pure GO, the CV, EIS, and GCD measurements are performed using the GO-CQDs composite synthesized with the optimal conditions (the reaction temperature of 150 °C, the calcination time of 120 min, and the m_{GO}:m_{CQDs} of 50:1).

Figure 6 shows the CV curves of GO and GO-CQDs electrodes measured in a three-electrode cell with scan rates of 10–1500 mV s^{-1}. Significant oxygen reduction peaks appear at about 0.3 V for both electrodes, and a pair of reversible peaks are found on the curve. The peak current (I_P) and ΔE_P measured at different scan rates from the CV curves are shown in table 1. When the scan rate increases from 10 to

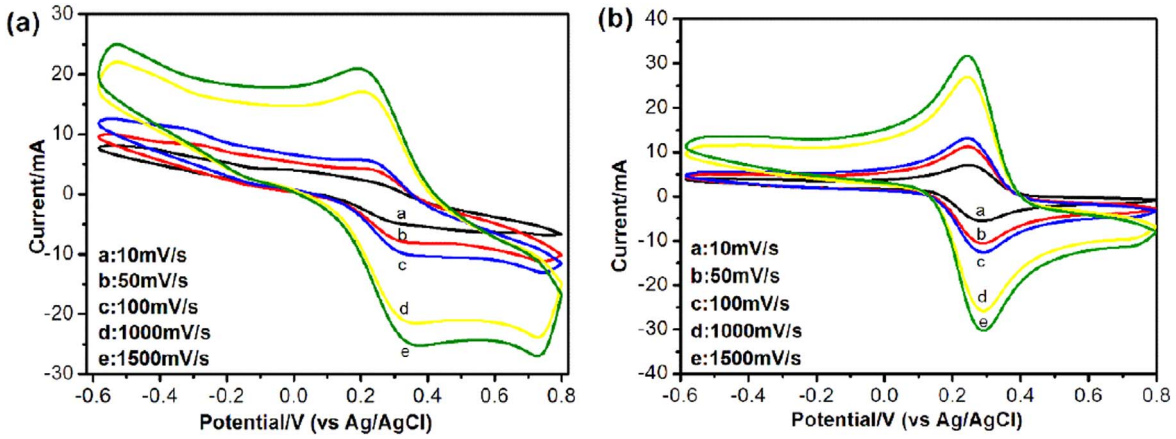

Figure 6. Cyclic voltammetry curves of (a) GO and (b) GO-CQDs electrodes at scan rates of 10–1500 mV s^{-1} in a mixture of 5 μM $K_3Fe(CN)_6$ and 1 M KCl.

Table 1. I_P and ΔE_P of GO and GO-CQDs electrodes measured by CV at various scan rates.

Scan rate (mV s^{-1})	GO		GO-CQDs	
	I_P (mA)	ΔE_P (mV)	I_P (mA)	ΔE_P (mV)
10	2	87	7.6	29
50	4.2	94	11	41
100	5.7	112	13.2	47
1000	17.1	124	27	48
1500	21	126	31.8	49

1500 mV s^{-1}, I_P of the GO electrode gradually increases from 2 to 21 mA, and that of the composite electrode increases from 7.6 to 31.8 mA. At the same scan rate, the I_P of the composite electrode is larger than that of the GO electrode. At the same voltage, the higher value of I_P leads to the higher capacitor power. In addition, at the same scan rate, ΔE_P of the composite electrode is smaller than that of the GO electrode, suggesting the better reversibility and electrochemical activity of the composite electrode. It indicates the GO-CQDs composites can be used to fabricate high performance biosensors.

Figure 7 shows the EIS spectra of the GO and GO-CQDs electrodes. Both two curves have a semicircle and a diagonal line controlled by charge transfer and diffusion, respectively. The radius of the semicircle in the high-frequency region reflects the magnitude of the charge transfer resistance. The diagonal line in the low-frequency region is caused by the Warburg impedance. The charge transfer resistance of the GO electrode is around 1.6 Ω, and that of the GO-CQDs electrode is smaller, about 0.9 Ω. The improved charge transfer of the GO-CQDs electrode compared with the bare GO could be attributed to the abundant electroactive sites provided by the CQDs. In addition, the straight lines of both the curves in the low-frequency region indicate that the charge transfer is controlled by the diffusion process after the electrolyte ions are transported to the surfaces of the two electrodes, which is consistent with the CV results.

3.4. Detection of UA and AA in GO-CQDs composites

Figures 8(a)–(d) show the CV curves of the GO-CQDs electrode measured in the PBS with different additions of UA and AA to test the selectivity of the electrode in detection of UA and AA. The CV curve of the GO-CQDs electrode in the PBS (figure 8(a)) is a standard rectangle with no redox peak, indicating that the GO-CQDs electrode can be used to detect signal molecules unaffected by the buffer solution.

When the buffer solution contains 1 mM AA (figure 8(b)), an obvious oxidation peak appears in 204 mV, indicating the composite electrode can be used to detect AA. A similar oxidation peak appears in 544 mV when the buffer solution contains 0.1 mM UA (figure 8(c)), therefore the composite electrode can be used to detect UA as well. The difference of oxidation peak positions is 340 mV when the AA and UA were detected separately.

The CV curve measured in a mixture of the PBS, 1 mM AA, and 0.1 mM UA (figure 8(d)) exhibits the capability of the GO-CQDs electrode to simultaneously detect UA and AA in the mixed solution. The characteristic oxidation peaks of the two molecules are observed at 204 mV and 542 mV, respectively, and the potential difference is 338 mV, which is only 2 mV smaller than the value measured separately (340 mV). Above indicates that the GO-CQDs composite electrode is sufficient to realize the selective detection of AA and UA.

Figure 9(a) is the DPV diagram of the GO-CQDs electrode in 0.1 M PBS containing 1 mM AA and 0.1–150 μM UA. There are two peaks at around 0.1 and 0.4 V, corresponding to AA and UA, respectively. Obviously, the peak current of UA increases with the UA concentration, while the peak current of AA basically remains unchanged as the concentration of AA in the solution is a constant (1 mM). Hence, the detection of UA is not interfered by the presence of AA, and the GO-CQDs electrode can be used to achieve a good selective detection of UA. Figure 9(b) is the linear fitting curve of the UA concentration versus the peak current in DPV. The

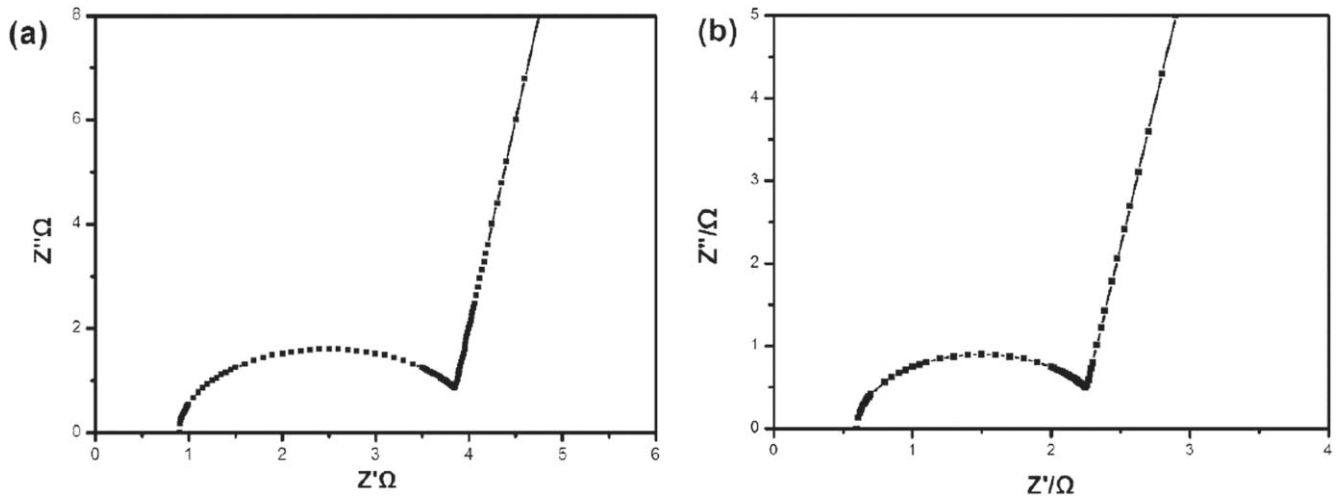

Figure 7. EIS spectra of (a) GO and (b) GO-CQDs electrodes.

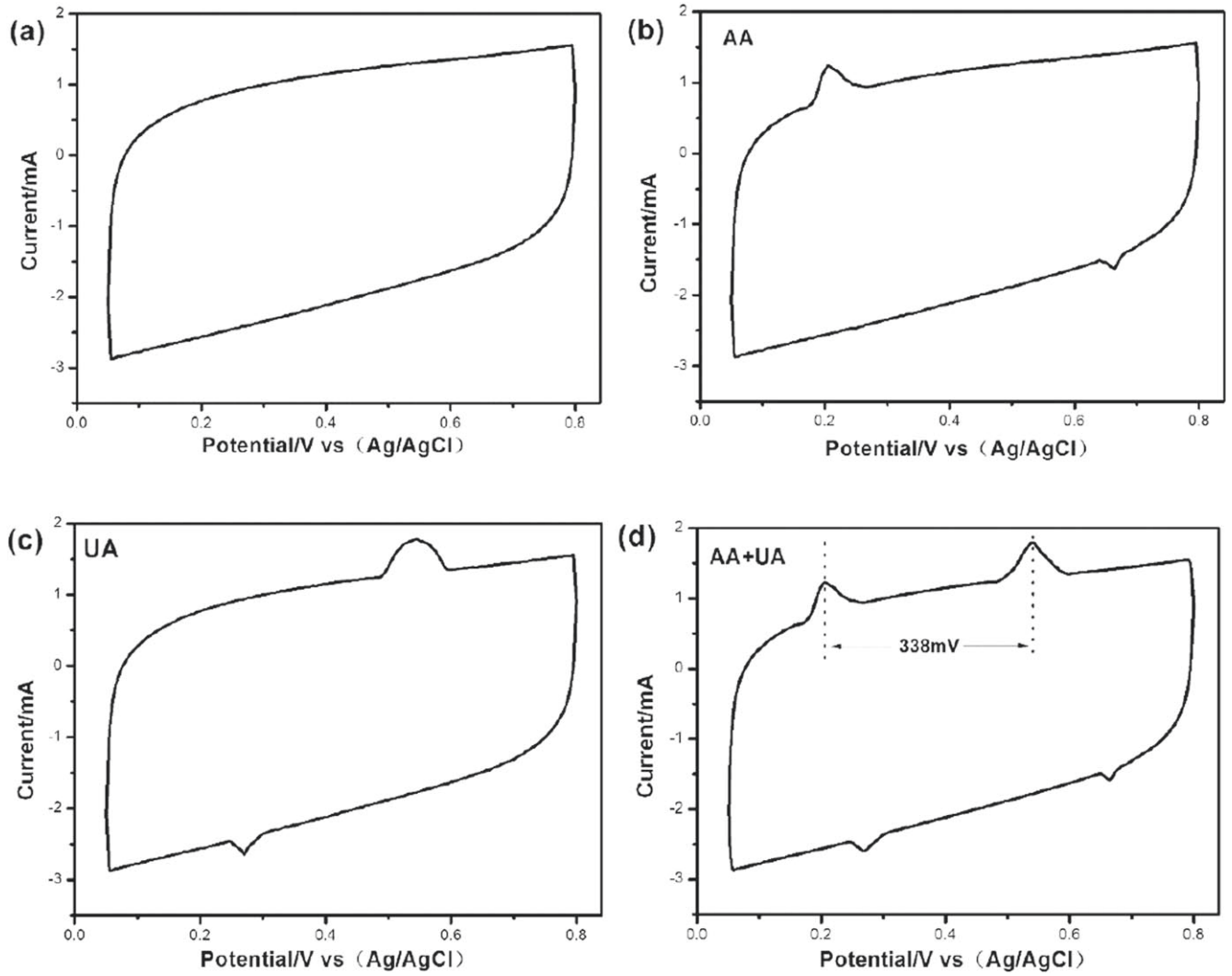

Figure 8. CV curves of the GO-CQDs electrode measured in (a) 0.1 M PBS, (b) 1 mM AA, (c) 0.1 mM UA, and (d) the mixture of 1 mM AA and 0.1 mM UA at a scan rate of 100 mV s^{-1}.

statistically significant correlation coefficient (R^2) is 0.9988, indicating an apparent electrochemical response of the GO-CQDs electrode to UA. It means that the concentration of UA can be mathematically reflected by the DPV peak current measured by the GO-CQDs electrode, even with the presence of 1 mM AA.

To accurately measure the minimum detection limit of UA and AA using the GO-CQDs electrode, the direct

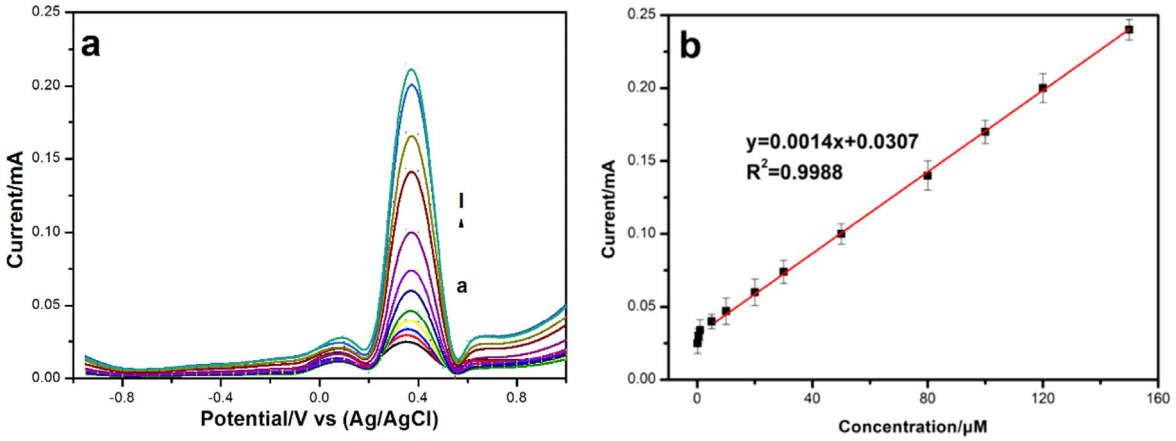

Figure 9. (a) DPV curves of the GO-CQDs electrode in 1 mM AA and 0.1 M PBS with 0.1, 0.5, 1, 5, 10, 20, 30, 50, 80, 100, 120, and 150 μM UA (from curve *a* to *l*); (b) the linear relationship between the UA concentration and DPV current.

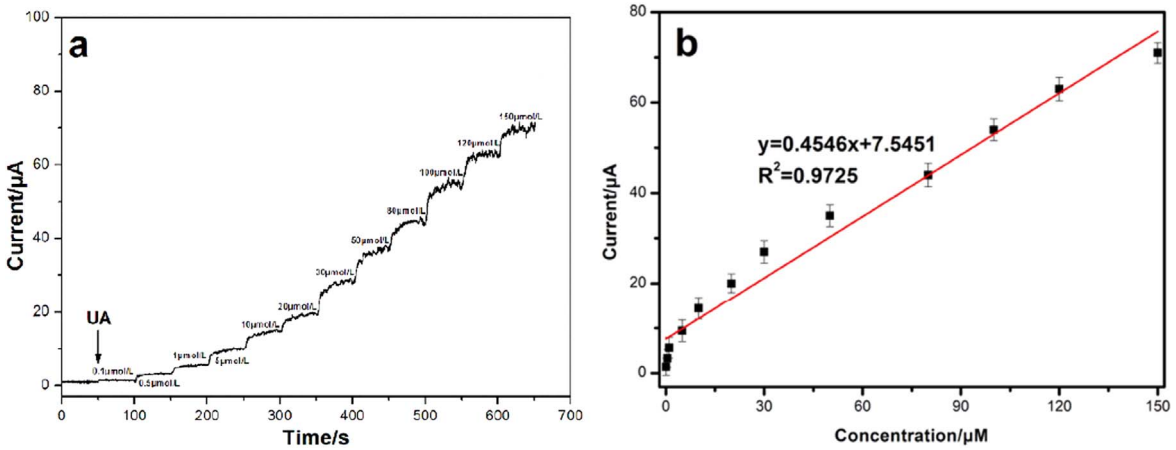

Figure 10. (a) Amperometric current–time responses of the GO-CQDs electrode under the continuous addition of UA with concentrations of 0.1, 0.5, 1, 5, 10, 20, 30, 50, 80, 100, 120, and 150 μM in 0.1 M PBS; (b) the linear relationship between the UA concentration and response current.

correlation between the UA and AA concentration and response current is explored. Figure 10(a) shows the amperometric current–time responses of the GO-CQDs electrode under the continuous addition of UA with concentrations of 0.1–150 μM in 0.1 M PBS at a voltage of 0.4 V. The response current increases with the UA concentration, and the step-state distribution is well aligned, further indicating that the GO-CQDs electrode has good stability in detecting UA. In addition, when the UA concentration as small as only 0.1 μM, a distinct current change from 0.8 to 1.4 μA can still be observed, indicating a very high sensitivity as well as a very low detection limit. The limit of detection (LOD) of GO-CQDs composite electrode for UA can be calculated to be 0.01 μM, based on the signal-to-noise ratio (S/N = 3). The LOD and detection range of this fabricated GO-CQDs sensors were comparable to those of previous electrochemical sensors for UA determination (table 2). In fact, using these data, the sensitivity and detection limit values can be calculated based on the corresponding formula reported in the literature [30].

Figure 10(b) shows the linear relationship between the UA concentration (μM) and response current (μA). The statistically significant correlation coefficient (R^2) is 0.9725, indicating a good linear correlation. The linear range of the GO-CQDs electrode for UA detection is 1–150 μM. The slope is calculated as 0.4546 μA μM^{-1}. Since the effective area of the electrode is 0.196 cm^2, the sensitivity of the GO-CQDs electrode for UA is 2319.4 μA mM^{-1} cm^{-2}. It can be seen that the sensitivity of 0.4546 μA μM^{-1} for UA is higher with the previously reported results (0.14 μA μM^{-1}) [36].

Similarly, figure 11(a) shows the amperometric current–time responses of the GO-CQDs electrode under the continuous addition of AA with concentrations of 800–9000 μM in 0.1 M PBS at a voltage of 0.4 V. The same well-aligned step-state distribution is found, indicating that the GO-CQDs electrode has good stability in detecting AA as well. The LOD of GO-CQDs electrode for AA can be calculated to be 31.57 μM. Figure 11(b) shows the linear relationship between AA concentration (μM) and response current (μA) with the statistically significant correlation coefficient (R^2) of 0.9993. The linear range of the GO-CQDs electrode for AA detection is 800–9000 μM. The slope is calculated as 0.0104 μA μM^{-1}. Since the effective area of the electrode is 0.196 cm^2, the sensitivity of the GO-CQDs electrode for AA is 53.1 μA mM^{-1} cm^{-2}. The LOD and detection range of this fabricated GO-CQDs sensors were comparable to those of

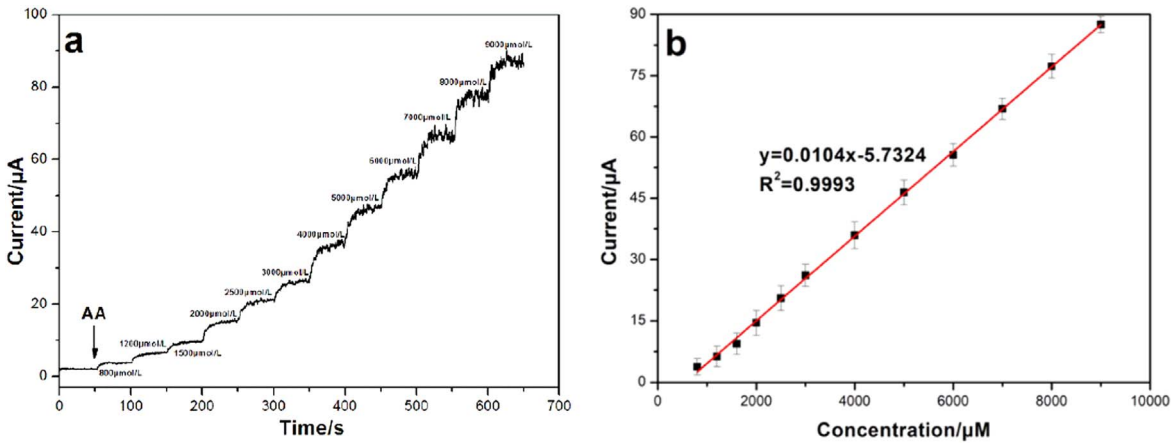

Figure 11. (a) Amperometric current–time responses of the GO-CQDs electrode under the continuous addition of AA with concentrations of 800, 1200, 1600, 2000, 2500, 3000, 5000, 6000, 7000, 8000, and 9000 μM in 0.1 M PBS; (b) the linear relationship between the AA concentration and response current.

Table 2. Comparison of different graphene-based electrochemical sensors for AA and UA determination.

Material	Transducer	LOD (μM)		Detection range (μM)		References
		AA	UA	AA	UA	
Au-Ag NPs/GO/TH	SWV	—	0.3	—	1–100	[14]
polyimidazole-GO	DPV	18	0.59	75–2275	3.6–249.6	[31]
Pt NPs/rGO	DPV	—	0.24	—	10–130	[32]
Graphene nanoflower -carbon fibers	DPV	73.5	3.98	73.5–2305	4.0–371.5	[33]
PVP-GR	SDLSV	0.8	0.02	40–1000	1–100	[34]
N-rGO	DPV	9.6	0.2	100–4000	1–30	[35]
GO-CQDs	DPV	31.57	0.01	800–9000	1–150	This work

previous electrochemical sensors for AA determination (table 2). It also indicates that obtained sensitivities are significantly comparable and better than some of the previous electrochemical sensors used for the determination of AA and UA [36, 31–35].

In addition, to compare the electrochemical performance of the electrodes modified with different kinds of carbon nanomaterials, we also researched the electrochemical performance of the electrodes modified with graphene-CQDs composites. The results were listed in Supplementary Materials (see figures S1 and S2 (available online at stacks.iop.org/NANO/32/135501/mmedia)). Compared with the GO-CQDs electrode, the electrochemical response (peak current, peak potential and correlation coefficient) of the graphene-CQDs electrode to UA were lower than that of GO-CQDs electrode. The reason may be that the graphene without functional groups is very stable and difficult to combine with CQDs. However, GO has a large number of functional groups on its surface, such as carboxyl, hydroxyl, and epoxy groups, which make it easy to bind to CQDs. The synergizing effect of GO and CQDs improved the electrochemical performance of the GO-CQDs electrode.

3.5. UA detection performance of the GO-CQDs electrode in biological samples

To evaluate the feasibility of this GO-CQDs electrode for UA determination, the sensor was used to analyze five serum and urine samples, and the results were consistent with the spectrophotometric method of Wuhan University of Science and Technology hospital (see table 3), indicating that the sensor could be used for the analysis of real samples.

Table 3. Determination of uric acid in human blood and urine samples.

Sample[a]	Found[b] (μM)	SD (%, n = 3)	Data from hospital (μM)
Serum 1	2.93	3.41	2.94
Serum 2	3.37	3.03	3.37
Urine 1	3.49	4.02	3.48
Urine 2	4.10	3.16	4.08
Urine 3	4.43	4.18	4.45

[a] Real human serum and urine fluids were 100-fold diluted with PBS (0.1 mM, pH 7.4).
[b] Obtained results were expressed as the average of three determinations standard deviation (SD).

The reproducibility of GO-CQDs modified electrode was investigated. Six electrodes prepared under the same conditions were used to detect 0.030 mM UA. The relative standard deviation of electrochemical signal was 4.1%. The RSD of the same electrode for the same sample was 3.8%, and the stability of the electrode was also investigated. The modified electrode was stored in a refrigerator at 4 °C. The results

showed that the electrochemical signal remained relatively unchanged after 2 weeks.

The above experimental results show that the modification of GO and CQDs on the surface of glass carbon electrode can greatly improve the conductivity and biocompatibility of the electrode and become a good bioelectrochemical platform due to the synergizing effect of GO and CQDs.

4. Conclusion

The GO-CQDs composites are synthesized using GO as the conductive skeleton to load CQDs by a one-step calcination method. The GO-CQDs composites with a mass ratio of GO to CQDs of 50:1 and heated at 150 °C for 60 min exhibits the best electrocatalytic activity and reversibility among all the samples. The morphological characteristics of GO-CQDs composites are similar to that of bare GO, but the crumpling and folding issues of GO in the GO-CQDs composites are improved. Compared with bare GO, the number of holes and defect sites of GO in the GO-CQDs composites is reduced, and therefore the graphitization degree of the composites is higher, reducing the lamellar stacking distance between the GO layers.

The electrochemical properties of the GO-CQDs composites as electrochemical sensors for the detection of UA and AA are studied. The results show that the linear range, minimum detection limit, and sensitivity of the GO-CQDs electrode for uric acid detection are 1–150 μM, 0.01 μM, and 2319.4 μA mM^{-1} cm^{-2}, respectively, and those for ascorbic acid detection are 800–9000 μM, 31.57 μM, and 53.1 μA mM^{-1} cm^{-2}, respectively. The GO-CQDs composites show great application prospects as electrochemical sensors.

In summary, it is found that the electrochemical properties of GO-CQDs composites are superior to that of bare GO. The great property improvement is attributed to the unique microstructure of the GO-CQDs composite, which integrates the two-dimensional GO as a conductive skeleton with zero-dimensional CQDs as an electroactive material to obtain composites with three-dimensional electron transport channels. This composite structure maintains the physical properties and electrical properties of the respective materials, has abundant binding sites for the electroactive substances, enhances the electron transfer capacity, and improves the electron transfer rate, which promotes the electrochemical activity of the composite material in comparison to the bare GO. This GO-CQDs sensor enabled efficient detection of UA in real human urine and serum samples. The experimental results testified that the as-developed GO-CQDs sensor had high practicability for biological molecule determination.

Acknowledgments

We gratefully acknowledge the financial support of the National Nature Science Foundation of China (51972242), the Opening Project of Key Laboratory of Optoelectronic Chemical Materials and Devices, Ministry of Education, Jianghan University (JDGD202017), the Open Fund of the Hubei Provincial Key Laboratory for New Processes of Ironmaking and Steel making (Wuhan University of Science and Technology) of China (KF-20-5), the Natural Science Foundation of Hubei Province (2017CFB680), the Open Fund of the State Key Laboratory of Refractories and Metallurgy (Wuhan University of Science and Technology) of China (G201703), Guiding Projects in Fujian Province (2018H0013) and the Opening Foundation of Henan Provincial Engineering Laboratory of Coal-based Ecological Fine Chemicals (C202006).

Declaration of competing interest

The authors declare that they have no known competing financial interests or personal relationships that could have appeared to influence the work reported in this paper.

ORCID iDs

Ling Ding https://orcid.org/0000-0002-4871-2352

References

[1] Ensafi A A, Ahmadi N and Rezaei B 2017 *Sensors Actuators* B **239** 807–15
[2] Fan G Y and Huang W J 2014 *Chin. Chem. Lett.* **25** 359–63
[3] Gao F, Cai X L, Wang X, Gao C, Liu S L, Gao F and Wang Q X 2013 *Sensors Actuators* B **186** 380–7
[4] Wang Z H, Guo H J, Gui R J, Jin H, Xia J F and Zhang F F 2018 *Sensors Actuators* B **255** 2069–77
[5] Xie L Q, Zhang Y H, Gao F, Wu Q A, Xu P Y, Wang S S, Gao N N and Wang Q X 2017 *Chin. Chem. Lett.* **28** 41–8
[6] Zhao D Y, Yu G L, Tian K L and Xu C X 2016 *Biosens. Bioelectron.* **82** 119–26
[7] Wang D L, Xu F, Hu J J and Meng L 2017 *Mater. Sci. Eng.* C **71** 1086–9
[8] Morresi T, Binosi D, Simonucci S, Piergallini R, Roche S, Pugno N M and Taioli S 2020 *2D Mater.* **7** 041004
[9] Sheng X X, Cai W X, Zhong L, Xie D L and Zhang X Y 2016 *J. Mater. Chem.* A **55** 8576–85
[10] Jiang Y Y, Tan Z Q, Fan G L, Zhang Z B, Xiong D B, Guo Q, Li Z Q and Zhang D 2020 *Carbon* **161** 17–24
[11] Morales-Narváez E and Merkoçi A 2019 *Adv. Mater.* **31** 1805043
[12] Jiang H, Lee P S and Li C Z 2013 *Energy Environ. Sci.* **6** 41–53
[13] Lv H P, Yuan Y, Xu Q J, Liu H M, Wang Y G and Xia Y Y 2018 *J. Power Sources* **398** 167–74
[14] Gao X H, Gui R J, Xu K Q Z, Guo H J, Jin H and Wang Z H 2018 *New J. Chem.* **42** 14796–804
[15] Wang Y, Yao H B, Wang X H and Yu S H 2011 *J. Mater. Chem.* **21** 562–6
[16] Gao N N, Gao F, He S Y, Zhu Q H, Huang J F, Tanaka H and Wang Q X 2017 *Anal. Chim. Acta* **951** 58–67
[17] Yao S, Hu Y F and Li G K 2014 *Carbon* **66** 77–83
[18] Ding L, Peng Z Z, Zhou P J, Cheng G J, Nian Q, Lin D, Zhou J H and Liang Y H 2015 *J. Fluoresc.* **25** 1663–9
[19] Wang L, Zhang X H, Yang K, Wang L N and Lee C S 2020 *Carbon* **160** 298–306

[20] Zhu S J, Meng Q N, Wang L, Zhang J H, Song Y B, Jin H, Zhang K, Sun H C, Wang H Y and Yang B 2013 *Angew. Chem., Int. Ed.* **52** 3953–7
[21] Zheng L Y, Chi Y W, Dong Y Q, Lin J P and Wang B B 2009 *J. Am. Chem. Soc.* **131** 4564–5
[22] Sun H J, Wu L, Wei W L and Qu X G 2013 *Mater. Today* **16** 433–422
[23] Hong T Z, Xue Q, Yang Z Y and Dong Y P 2016 *J. Power Sources* **303** 109–17
[24] Hummers W S and Offeman R E 1958 *J. Am. Chem. Soc.* **80** 1339
[25] Xiao H, Zhang J J, Zhao M, Ma J C, Li Y, Hu T J, Zheng Z F, Jia J F and Wu H S 2020 *J. Power Sources* **451** 227770
[26] Zhang Q G, Liu H C, Zhang X Y, Li M C and Jin Z X 2014 *Electron Compon. Mater.* **33** 29–32
[27] Xu L, Yang L, Bai X, Du X Y, Wang Y and Jin P K 2019 *Chem. Eng. J.* **373** 238–50
[28] Lightcap I V and Kamat P V 2012 *J. Am. Chem. Soc.* **134** 7109–16
[29] Zhou L, Liu J, Zhang X, Liu R H, Huang H, Liu Y and Kang Z H 2014 *Nanoscale* **6** 5831–7
[30] Muthurasu A and Ganesh V 2014 *Appl. Biochem. Biotechnol.* **174** 945–59
[31] Liu X, Zhang L, Wei S, Chen S, Ou X and Lu Q 2014 *Biosens. Bioelectron.* **57** 232–8
[32] Xu T, Zhang Q, Zheng J, Lv Z, Wei J, Wang A and Feng J 2014 *Electrochim. Acta* **115** 109–15
[33] Du J, Yue R, Ren F, Yao Z, Jiang F, Yang P and Du Y 2014 *Biosens. Bioelectron.* **53** 220–4
[34] Wu Y Y, Deng P H, Tian Y L, Feng J X, Xiao J Y, Li J H, Liu J, Li G L and He Q G 2020 *J. Nanobiotechnol.* **18** 112
[35] Zhang H Y and Liu S 2020 *J. Alloys Compd.* **842** 155873
[36] Aryal K P and Jeong H K 2020 *Chem. Phys. Lett.* **739** 136969